Macromolecules

ARTICLE

pubs.acs.org/Macromolecules

Polymorphism and Structural Transition around 54 °C in Regioregular Poly(3-hexylthiophene) with High Crystallinity As Revealed by Infrared Spectroscopy

Yuan Yuan, Jianming Zhang,* Jiaqian Sun, Jian Hu, Tongping Zhang, and Yongxin Duan*

Key Laboratory of Rubber-Plastics, Ministry of Education/Shandong Provincial Key Laboratory of Rubber-plastics, Qingdao University of Science & Technology, Qingdao City 266042, People's Republic of China

ABSTRACT: Poly(3-hexyllthiophene) (P3HT) with high crystallinity was prepared by controlling the solvent evaporation rate together with the aid of chloroform vapor annealing. According to the infrared spectroscopy combined with the thermal analysis and the X-ray diffraction (XRD) data, a new crystal modification named as form I′ was identified for P3HT sample crystallized under extremely slow evaporation rate at low temperature (13 °C). Such crystal modification has shorter interlayer distance than that of the more common but more disordered form I of P3HT. Moreover, it demonstrates a distinct endothermic peak around 54 °C and a characteristic IR band at 823 cm^{-1}, which have never been reported for P3HT in the literature. The origin of the structural transition around 54 °C is investigated in detail by temperature-dependent infrared spectroscopy combined with the *in situ* synchrotron WAXD measurement. It is found that, during the heating process of P3HT form I′ crystal, there is the form I′-to-form I phase transition from 30 to 60 °C, which belongs to the solid-to-solid phase transition.

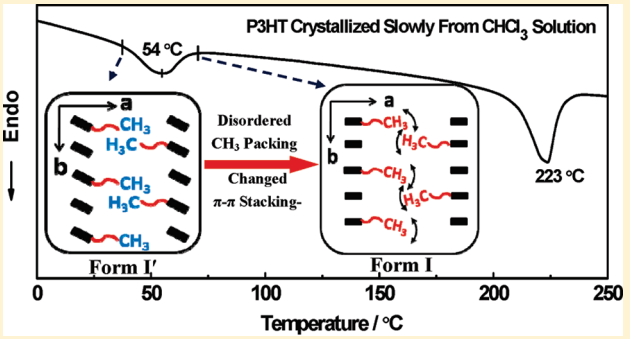

1. INTRODUCTION

Among the family of regioregular poly(3-alkylthiophene) (P3AT), poly(3-hexylthiophene) (P3HT) is the most-used conjugated polymer in organic electronic applications due to its better balance between the solubility and electric properties.[1−4] Intensive research toward improving its mobility has shown that the microstructure in P3HT is critically affected by regioregularity,[5] molecular weight,[6] and sampling methods,[7,8] resulting in variation of the field-effect mobility by several orders of magnitude.[9]

Compared to the linear polymer, the comb-like P3AT in general demonstrates more complex hierarchical equilibrium structure. Although extensive structural analysis has been performed on the condensed structure of P3HT during the past decades, it is found that further refinements are required for an accurate description to the crystal structure of P3HT. Especially, there are open questions on the ordering of the alkyl side chains and $\pi-\pi$ stacking modes in the P3HT crystal. Very recently, by studying the crystal structure and the phase transition behavior of bulk P3HT, two intriguing viewpoints were proposed.[3,10,11] One is that the side-chain crystallization and melting can take place in P3HT. Usually, it is thought that crystallization within the alkyl nanodomains of comblike polymers often occurs just for side chains containing more than 10 alkyl carbons.[12−15] However, Pankaj et al.[10] recently reported that there are side-chain crystallization even for regiorandom P3AT containing 6−12 alkyl carbons per side chain. By temperature-dependent WAXD measurement of regioregular P3HT with well-defined molecular weight, Thelakkat et al.[3] observed that several (hk0) diffractions start to disappear with increasing temperature above 60 °C, and they proposed that the disappearing of these (hk0) diffractions was attributed to the "melting of hexyl side chains". The other novel viewpoint is that, with the detailed structure refinement based on electron diffraction from epitaxial thin films, Brinkmann et al.[11] proposed that the stacking period of successive P3HT backbones along the b-axis is 0.39 nm, but a short interplanar distance of 0.34 nm is observed due to the tilted chain packing. Such suggestion means that the $\pi-\pi$ stacking or $\pi-\pi$ interaction in P3HT crystal is much stronger than ever thought. On the basis of ab initio density functional calculations, Dag et al. also found that the low-energy and thermodynamically stable P3HT stacking structure is a tilted structure with such short $\pi-\pi$ stacking of 0.34 nm.[16] Of note, the structural model of P3HT proposed by Brinkmann et al. also suggests that the n-hexyl side groups crystallize in an orthogonal subcell with parameters a_s = 0.7 nm and b_s = 0.78 nm.[11] Nevertheless, direct experimental evidence for supporting these novel ideas on the crystalline structures of P3HT is very lacking at the current stage.

Stimulated by these open questions, we studied the effect of chloroform evaporation rate on the crystalline structure and the thermal behavior of the final obtained bulk P3HT samples by combining the thermal analysis (DSC), wide-angle X-ray diffraction technique (WAXD), and temperature-dependent infrared

Received: July 25, 2011
Revised: September 26, 2011
Published: November 03, 2011

Scheme 1. Illustration of Sampling Process for (a) Fast Evaporated Film (P3HT-FE) and (b) Slowly Evaporated Film (P3HT-SE)

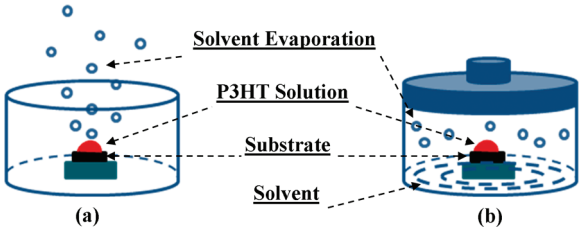

spectroscopy (FTIR). It is found that the slow solvent evaporation rate at low temperature (13 °C) not only improves the crystallinity but also enhances the ordering of the final crystalline structure, which actually leads to a new crystal modification named as form I′. During the heating process, the form I′ crystal is transformed to the conventional form I around 54 °C. The phase transition mechanism and the associated changes of the packing structure concerning the side chains and the conjugated planes were revealed and discussed based on the temperature-dependent IR spectra, which is a local technique and sensitive to the chain conformation and interchain packing of semicrystalline polymer. Our result is another evidence to confirm that the microstructure,[7,8] especially the stacking structures in P3HT, is critically affected not only by the sampling conditions but also by the subsequently thermal annealing process. Also, it is expected that our research will accumulate some experimental evidence and provide new insights into understanding the hierarchical structures of P3HT.

2. EXPERIMENTAL SECTION

2.1. Material and Sample Preparation Procedure. Regioregular poly(3-hexylthiophene) (P3HT) (#4002-E, M_w = 4.56 × 10^4 g/mol and M_n = 2.01 × 10^4 g/mol, regioregularity is 90−94%) was purchased from Rieke Metals, Inc. It was first dissolved in chloroform (concentration 20 mg/mL) and stirred on a hot stage at 40 °C until complete dissolved. Then, the extremely slow crystallized P3HT film was prepared by casting several drops of solution on a substrate, which was put inside a cylinder container with a radius and height of 1.5 and 3 cm, respectively. Meanwhile, several chloroform drops were deposited around the substrate to generate chloroform partial pressure. By sealing the container with a lid immediately and then keeping the container in refrigerator under the temperature of 13 °C, the very slow solvent evaporation rate can be obtained, and it took ca. 24 h for the film to dry. The sample obtained in such way was named as "P3HT-SE". For comparison, as-cast sample with fast solvent evaporation rate in an open container without lid at room temperature was also prepared, and it was named as "P3HT-FE". The different sampling methods for "P3HT-SE" and "P3HT-FE" are illustrated in Scheme 1. After the majority of solvent had been evaporated and the films turned to dry, the samples were then placed under vacuum at room temperature for 24 h to remove residual solvent completely. The as-prepared film thickness is about 20 μm.

2.2. Differential Scanning Calorimetry (DSC). DSC measurement was performed on a TA Q20 calorimeter system under flowing nitrogen gas at a heating rate of 10 °C/min. About 3 mg sample was sealed in aluminum pan and equilibrated at −50 °C prior to measurement.

2.3. Wide-Angle X-ray Diffraction (WAXD). The measurement of WAXD in reflection mode was performed using the Rigaku SmartLab X-ray Diffractometer with Cu Kα radiation (λ = 0.154 nm). WAXD patterns were taken in the 2θ range from 2° to 30° by continuous scanning with a step size of 0.05°.

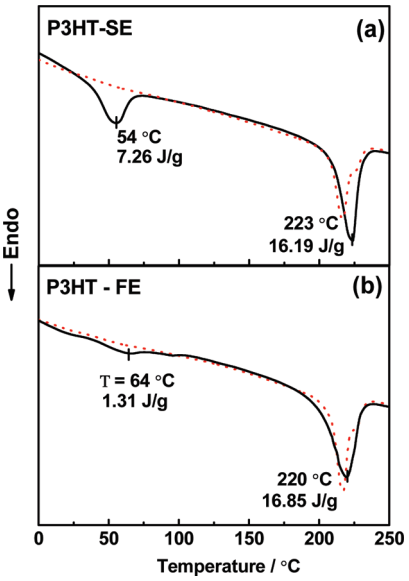

Figure 1. DSC heating curves of slowly crystallized sample (P3HT-SE) (a) and as-cast sample (P3HT-FE) (b) from $CHCl_3$ solution. The second heating curves of P3HT-SE and P3HT-FE are also shown as dotted lines in (a) and (b), respectively.

The temperature-dependent WAXD measurement in transmission mode was performed at the BL 40B2 beam station at Sping-8 (Japan Synchrotron Radiation Research Institute, Hyogo, Japan). The wavelength of the incident X-ray beam was 0.1 nm. A Rigaku R-AXIS IV ++ imaging plate system was used as the 2D detector. The sample was packed into an aluminum pan, which was set to a DSC cell (Metlar Toledo FP90). The X-ray exposure time was 20 ms for every WAXD measurement and the heating rate of 10 °C/min. In the heating process from −20 to 120 °C, the WAXD data were collected every ca. 0.7 °C. WAXD patterns measured were corrected for the background scattering.

2.4. FTIR Measurement and IR Data Treatment. FTIR spectra were measured with a Bruker tensor 27 spectrometer equipped with a DTGs detector. The normal transmission mode was employed for IR measurement. For studying the thermal behavior of P3HT via *in situ* FTIR, the as-prepared film on KBr substrate was set on a Harrick variable temperature cell, which was placed into sample compartment of the spectrometer. Subsequently, the sample was heated at a 2 °C/min from room temperature to 250 °C in a nitrogen atmosphere. During the heating process, FTIR spectra of the specimen were recorded at a 1 min interval from 30 to 250 °C. The spectra were obtained by coadding 16 scans at a 2 cm^{-1} resolution.

The intensities of IR bands were calculated automatically by a numerical data processor program for vibrational spectroscopy, Spina Version 3, which was developed by Yukiteru Katsumoto in the Ozaki Group of Kwansei-Gakuin University. Prior to the intensity calculation, all of the spectra were baseline corrected. Then, peak heights were calculated at fixed wavenumber for all spectra by this program.

3. RESULTS AND DISCUSSION

3.1. Thermal Behavior of Solution Cast P3HT Film with Different Solvent Evaporation Rate. Figures 1a and 1b show the first heating traces of the sample crystallized under the extremely slow solvent evaporation rate (P3HT-SE) and the as-cast one with the fast solvent evaporation rate (P3HT-FE),

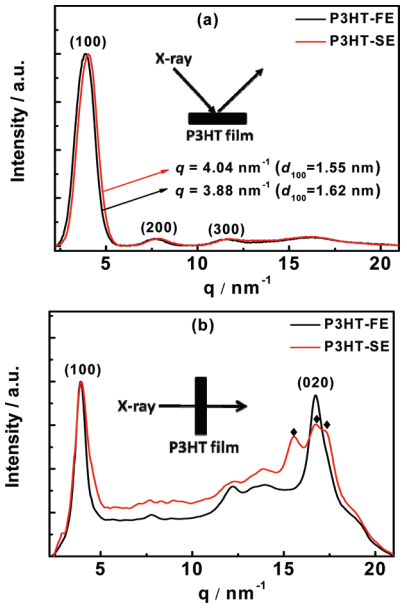

Figure 2. WAXD profiles measured in reflection mode (a) and in transmission mode (b) for slowly crystallized (P3HT-SE) and as-cast film (P3HT-FE). For comparison, the diffraction patterns are normalized using the strongest (100) diffraction intensity. Schematic representations for the WAXD modes are illustrated as inset graphs.

respectively. For comparison, their second heating curves are also shown as dotted lines in Figure 1. In the first heating traces, two endothermic peaks located at 54 °C (ΔH = 7.26 J/g) and 223 °C (ΔH = 16.19 J/g) are observed clearly for P3HT-SE, whereas only one obvious endothermic peak located at 220 °C (ΔH = 16.85 J/g) is identified for P3HT-FE. Both samples exhibit the same thermal behavior in their second heating curves, in which only one endothermic peak occurs around 190−230 °C.

Definitely, the endothermic behavior in the region of 190−230 °C shown in both samples should be associated with the melting process of P3HT crystal. To the best of our knowledge, such observation on the distinct endothermic peak located at 54 °C for commercial P3HT sample as used here has not been reported yet in the literature, although there is similar report for as-cast poly(3-butylthiophene) (P3BT) film.[17] It should be mentioned that Pascui et al. observed a subtle endothermic peak around 60 °C by investigating a series of regioregular P3HT with well-defined molecular weight (5−19 kg/mol).[18] However, by examining and comparing the data carefully, it should be pointed out that the phenomenon in their DSC data is more similar to the observation around 64 °C as indicated in Figure 1b for P3HT-FE rather than that for P3HT-SE.

Pascui et al. also reported that typical crystallinities are at least 37% for P3HT with the lowest molecular weight and as high as about 64% upon increasing molecular weight.[18] Moreover, they proposed that a corrected maximum value for the reference melting enthalpy of P3HT is $\Delta H_m^\infty \approx 37$ J/g.[18] According to this value, the crystallinity of P3HT-SE reaches to 63% by including the enthalpy value of the endothermic peak around 54 °C, whereas the crystallinity of P3HT-FE is as low as 49%. Generally, it will be not suitable to calculate the crystallinity of the initial sample just from the final melting enthalpy when there is structural changes or multiple melting behavior during the heating process;[19] we therefore added two endothermic peak together

Scheme 2. Schematic Models of the Form I (a) and Form II (b) Crystal Structure for rr-P3AT

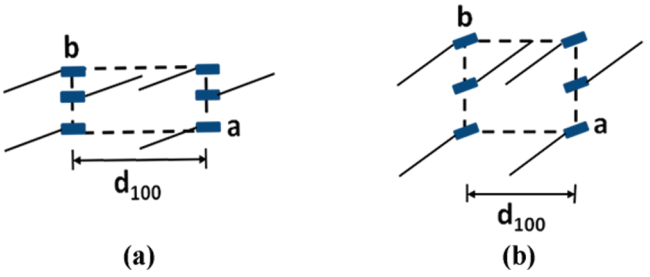

for the estimation of crystallinity. The calculated value based on DSC suggests that slower evaporation rate of chloroform does facilitate the growth of a highly crystalline film. The conclusion will be supported by the IR data later. Prior to exploring the origin of this endothermic peak around 54 °C, we first investigate the initial condensed structures of P3HT-SE and P3HT-FE.

3.2. Initial Crystal Structure at Room Temperature Investigated by WAXD and FTIR. Usually, P3AT chains could take the in-plane orientation in the solution-cast film. For investigating the structural difference between P3HT-FE and P3HT-SE in a comprehensive way, WAXD measurements in both reflection and transmission modes were performed, and the results are shown in Figures 2a and 2b, respectively. All of these data are measured at room temperature so that temperature factor can be precluded. As illustrated in Figure 2a, although the overall WAXD profiles of P3HT-FE and P3HT-SE are highly similar, a small peak shift for the (100) diffraction between them can be clearly observed. Such observation is further confirmed by the higher order (h00) diffraction peaks, such as suggested by the (200) and (300) peaks. It is found that the strongest (100) diffraction peaks located at q = 3.88 nm^{-1} (d_{100} = 1.62 nm) and q = 4.04 nm^{-1} (d_{100} = 1.55 nm) for the as-cast film and the slowly crystallized one, respectively. According to the widely accepted packing model for P3AT as shown in Scheme 2, π-conjugated polythiophene chains organize in planes separated by layers of alkyl side chains.[11,16,20] In general, the d_{100} spacing is defined to represent the interlayer distance between conjugated backbones. The difference in d_{100} spacing suggests that there is closer interlayer packing in sample P3HT-SE than that in P3HT-FE.

As a matter of fact, depending on molecular weight and sampling conditions, the values of d_{100} spacing are usually reported around 1.6 nm for form I in most cases,[21] whereas it is around 1.2 nm for form II of P3HT.[6] Zen et al. had found that, with increasing the molecular weight from $M_n = 2.5 \times 10^3$ to $M_n = 2.7 \times 10^4$ g/mol, the d_{100} interlayer distance increases from 1.57 to 1.73 nm.[6] In the present study, the molecular weight of our sample is relatively high ($M_n = 2.01 \times 10^4$ g/mol). Thus, the d_{100} = 1.55 nm for our as-prepared sample of P3HT-SE shows an unusual closer interlayer packing than the most common form I of P3HT, and it indicates that the crystal modification of slowly crystallized P3HT-SE may be different from the conventional form I and form II of P3HT.

In general, in the line of studying the difference of P3AT crystal modifications, both the a- and b-axes length should be examined.[17,20] However, due to the orientation factor, the detailed structural information along the b-axis direction that reflects the lateral $\pi-\pi$ stacking is missing as shown in Figure 2a.

dx.doi.org/10.1021/ma2017106 |Macromolecules 2011, 44, 9341–9350

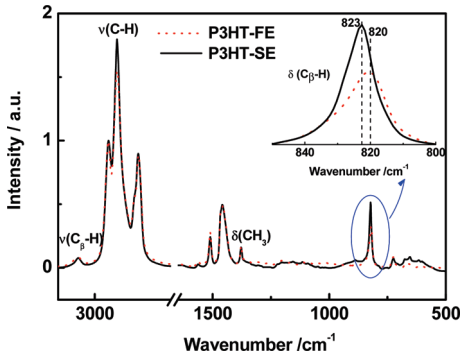

Figure 3. IR spectra of slowly crystallized P3HT film (P3HT-SE) and the as-cast film (P3HT-FE) in the region of 3100−500 cm^{-1}. Band at 1378 cm^{-1} was used as the normalized band. The inset graph shows the local spectra of the samples in the region of 850−800 cm^{-1}.

Scheme 3. Chemical Structure of P3HT[a]

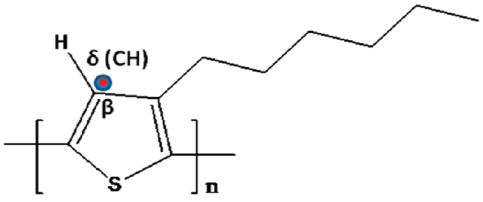

[a] The vibration direction of C_β−H out-of-plane deformation mode is indicated by the blue and red circle.

In order to check this point, WAXD measurement in transmission mode was also employed.

As denoted in Figure 2b, very strong diffraction peaks appear in the q region of 15−18 nm^{-1} for both the samples. Of note, the WAXD profile for P3HT-SE is quite different from that for P3HT-FE. That is, one diffraction peak located at q = 16.70 nm^{-1} is dominated for P3HT-FE, whereas three diffraction peaks can be identified for P3HT-SE. By comparing to the reported XRD data, the diffraction peak located at q = 16.70 nm^{-1} can be assigned to the (020) diffraction of P3HT form I crystal, with the $\pi-\pi$ stacking distance of 0.38 nm.[20−22] Currently, it is hard to index the multiple diffraction peaks for P3HT-SE due to there is no similar report in the literature. However, the obvious difference in diffraction patterns suggests that P3HT-SE take a new crystal modification, which is different from the traditional form I of P3HT.

To one's surprise, it can be seen that the transmission WAXD data for the two samples do not show obvious difference compared to reflection one for (100) peaks. This reason may be that the positions/shapes of the apparent (100) peaks, which are relatively weak in transmission mode, are affected by other low-angle diffractions from (0kl) planes. As shown in Figure 2b, the peak shapes of the (100) peaks are not so symmetry as those shown in Figure 2a, which indeed suggests that there is some contribution from other diffraction peaks.

More evidence to confirm the existence of the new P3HT modification can be revealed by infrared spectroscopy, which is sensitive to the local molecular packing in semicrystalline polymer. As shown in Figure 3, IR spectra measured at room temperature for as-cast P3HT film and the slowly crystallized one are presented. All these spectra were normalized by the intensity of the methyl deformation mode at 1378 cm^{-1}, which is used sometimes as internal standard band because the frequency and intensity of this vibration mode is generally not much sensitive to structural change.[23] It is found that notably spectral difference between as-cast film and the slowly crystallized one is mainly located in the 850−800 cm^{-1} region, which is dominated by the out-of-plane deformation modes of thiophene C_β−H.[24] As shown in the inset of Figure 3, the as-cast P3HT-FE and slowly crystallized P3HT-SE demonstrate characteristic bands at 820 and 823 cm^{-1}, respectively.

Table 1. Bands Assignment Related to the Structural Transition for P3HT

IR frequencies (cm^{-1})	assignments
3054	$\nu(C_\beta-H)$[a]
2955	$\nu_{as}(CH_3)$[a]
2870	$\nu_s(CH_3)$[a]
2859	$\nu_s(CH_2)$[a]
1510	$\nu_{as}(C=C)$[a]
1458	$\nu_s(C=C)$[a]
1378	$\delta(CH_3)$[a]
835	$\delta(C_\beta-H)$ in amorphous phase[a]
823	$\delta(C_\beta-H)$ in crystalline phase: form I′[b]
820	$\delta(C_\beta-H)$ in crystalline phase: form I[a]

[a] Assignments based on the report of references. [b] Our tentative assignment based on WAXD data.

The C_β−H out-of-plane deformation mode has been reported to be sensitive to the crystalline structure. For example, Yazawa et al. found that the characteristic bands at 820 and 835 cm^{-1} can be respectively assigned to form I crystal and the amorphous phase of P3HT.[24] Moreover, as depicted in the molecular structure of P3HT (see Scheme 3), this vibration mode is attached directly with the conjugated ring and its vibration is along the $\pi-\pi$ stacking direction. We therefore propose that the peak position of this vibration mode should be associated with the various stacking structures of conjugated rings. To the best of our knowledge, the characteristic band at 823 cm^{-1} is reported here for the first time. Although the difference between the band at 823 cm^{-1} for P3HT-SE and that at 823 cm^{-1} for P3HT-FE is not so notable, we think that such a difference is convincible due to the previous DSC and WAXD data suggest that there is obvious difference for these two samples. Thus, the IR data is another evidence for supporting the finding of a new crystal modification for P3HT.

By summarizing the observations discussed above, we tentatively name the so-called new crystal modification for P3HT-SE as form I′ because its WAXD data is close to that of P3HT form I. Moreover, it is thought that the crystalline structure of form I′ is more ordered than that of conventional form I. The reasons are as follows. First, there is shorter layer distance in form I′ than that in form I. Second, the characteristic crystalline band at 823 cm^{-1} for form I′ is sharper than that at 820 cm^{-1} for form I. Third, the notable endothermic peak in the DSC heating curve of P3HT-SE suggests that there is an order-to-disorder phase transition. This case reported here is highly similar to that of P3BT, in which form I′ recently proposed by Arosio et al. also presents some analogies but significant differences from the more disordered form I.[17] Combining our finding together with that of Arosio et al., we think that form I′ should be another universal crystal modification like the form I and form II of P3AT. For clarifying the difference

dx.doi.org/10.1021/ma2017106 |Macromolecules 2011, 44, 9341–9350

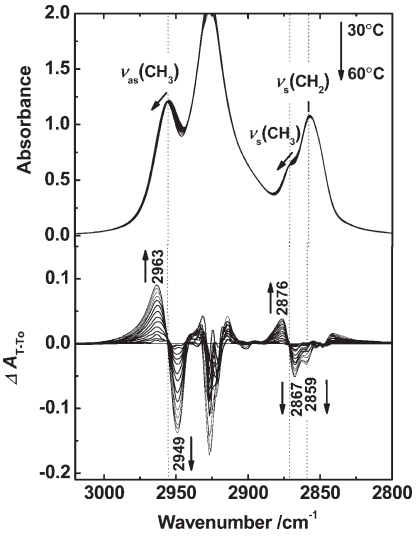

Figure 4. IR spectral changes in the C−H stretching vibration region from 30 to 60 at 2 °C intervals and the corresponding difference spectra obtained by the subtraction of the initial spectrum measured at 30 °C are shown in the up and down part, respectively.

between form I′ and form I furthermore, we performed the temperature-dependent IR measurement. The structural changes on the side chain packing and the $\pi-\pi$ stacking associated with this phase transition of form I′-to-form I will be mainly discussed.

3.3. Phase Transition in the Heating Process of Form I′ Investigated by Temperature-Dependent IR Spectroscopy. Most of the IR characteristic bands of P3HT have been well established in the literature, except that the assignment of band at 823 cm^{-1} to form I′ is based on our above analysis. As listed in Table 1, the C−H stretching vibration bands in the 3000−2800 cm^{-1} region is associated with alkyl side chain, whereas the stretching vibration mode in the 3080−3020 cm^{-1} region and the out-of-plane deformation modes in the 850−800 cm^{-1} region of thiophene C_β−H are attributed to the $\pi-\pi$ stacking, respectively.[22,25−27] Special attention will be paid in these spectral regions for analyzing the temperature-dependent IR spectra of the sample P3HT-SE in the following subsection.

3.3.1. Structural Changes Associated with Alkyl Side Chain Packing. 3000−2800 cm^{-1} Region: CH_2 and CH_3 Stretching Vibration Modes. The intensities of the bands in the 1400−1200 cm^{-1} region are generally used to monitor the conformational change of the P3AT alkyl side chains. However, considering that the conformation-sensitive bands in this region are very weak in intensities and they are heavily overlapped, we examined the spectral changes in the C−H stretching modes region, in which the CH_2 and CH_3 stretching bands demonstrate adequately strong intensities.

Figure 4 displays the spectral changes in the 3000−2800 cm^{-1} region from 30 to 60 °C, in which the endothermic peak located at 54 °C appears for the sample P3HT-SE. As shown in Figure 4, the intensity of $\nu_{as}(CH_2)$ at 2926 cm^{-1} is saturated due to we use thicker film for improving the intensities of some weaker bands. However, the intensities of the $\nu_s(CH_2)$, $\nu_s(CH_3)$, and $\nu_{as}(CH_3)$ modes are suitable for both the qualitative and quantitative analysis. As seen from the original spectra in Figure 4, a subtle peak shift toward higher frequencies can be discernible for the $\nu_s(CH_3)$ and $\nu_{as}(CH_3)$ bands located around 2870 and 2955 cm^{-1}, respectively. However, there is no obvious peak shift for the

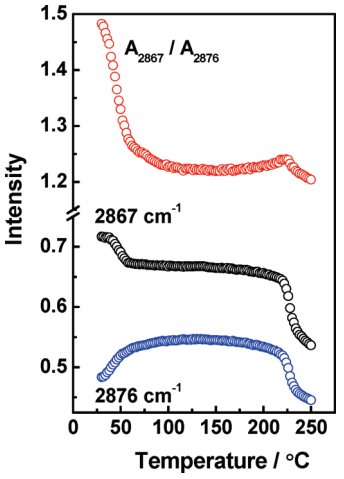

Figure 5. Intensity changes of the bands at 2867 and 2876 cm^{-1} and their intensity ratio A_{2867}/A_{2876} as a function of temperature.

$\nu_s(CH_2)$ band. Such spectral changes are presented more clearly in the corresponding difference spectra by the subtraction of the initial spectrum measured at 30 °C as depicted at the bottom of Figure 4. The appearance of a positive peak located at 2963 cm^{-1} and a negative peak located at 2949 cm^{-1} in the difference spectra contributes to the apparent peak shift of the $\nu_{as}(CH_3)$ band around 2955 cm^{-1} in the original spectra. A similar situation (positive peak at 2876 and negative peak at 2867 cm^{-1}) can be found for the $\nu_s(CH_3)$ band around 2870 cm^{-1}. However, the only negative peak in the difference spectra around 2859 cm^{-1} demonstrates that there is intensity decreasing but no peak shift for the $\nu_s(CH_2)$ band.

Usually, the bands shifting to higher wavenumber of C−H stretching mode suggests an increasing in the population of disordered conformation, that is, the gauche conformers. For example, the conformational disordering of an *all-trans*-polyethylene chain can be accompanied by an upward shift in the $\nu_s(CH_2)$ and $\nu_{as}(CH_2)$ band maxima by 2−3 and 5−7 cm^{-1}, respectively.[28,29] Herein, it is interesting to find that there is peak shift for the CH_3 stretching mode but not for the CH_2 stretching mode. This observation leads us to conclude that in the temperature region from 30 to 60 °C the packing of end CH_3 groups in form I′ experiences an obvious disordering process rather than the CH_2 stems in the hexyl side chains.

The intensities of the bands at 2876 and 2867 cm^{-1} as revealed by the difference spectra and their relative intensity (A_{2867}/A_{2876}) as a function of temperature from 30 to 250 °C are plotted in Figure 5. It is found that the intensity ratio of A_{2867}/A_{2876} decreases largely in the temperature region of 30 to 60 °C, whereas it is almost kept constant with further heating until the melting occurs. The distinct changes associated with the $\nu_s(CH_3)$ bands suggest that the ordered packing of end CH_3 groups in form I′ turns to disordered one in the temperature region from 30 to 60 °C, which is associated with the endothermic peak at 54 °C of P3HT form I′.

3.3.2. Structural Changes Associated with $\pi-\pi$ Stacking. 850−800 cm^{-1} Region: C_β−H Out-of-Plane Deformation Modes. Figure 6 shows temperature-dependent spectral changes of thiophene C_β−H out-of-plane deformation modes in the 850−800 cm^{-1} region. For illustrating the spectral changes with temperature more clearly, the spectra are displayed first in a stacked way at 4 °C intervals from 30 to 250 °C. With increasing

dx.doi.org/10.1021/ma2017106 |*Macromolecules* 2011, 44, 9341–9350

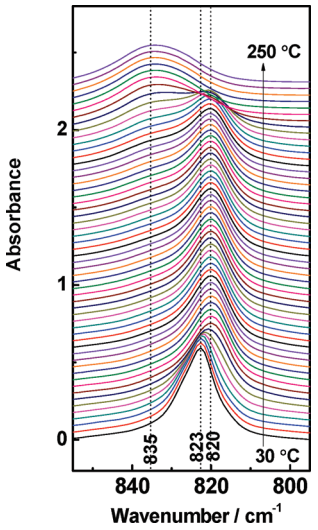

Figure 6. Temporal IR spectral changes in the C_β—H out-of-plane deformation band region during the heating process of the slowly crystallized P3HT from 30 to 250 at 4 °C intervals. These spectra are displayed in a stacked way.

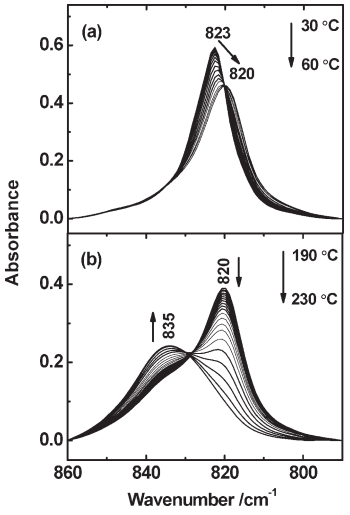

Figure 7. Overlapped IR spectral changes in Figure 6 from 30 to 60 °C (a) and from 190 to 230 °C (b) at 2 °C intervals.

temperature, three bands located at 823, 820, and 835 cm^{-1} sequentially dominate the spectral region of 850—800 cm^{-1}. According to our previous analysis, the bands at 823 and 820 cm^{-1} are respectively assigned to the form I′ and form I modifications for P3HT, whereas the band at 835 cm^{-1} should be undoubtedly associated with the amorphous phase because it is dominant above the P3HT melting temperature.

Spectral changes of these bands in the temperature region of 30—60 °C (associated with the endothermic peak around 54 °C as shown in Figure 1a) and 190—230 °C (melting region) are shown in Figures 7a and 7b, respectively. In the temperature region of 30—60 °C, it is found that the band at 823 cm^{-1} decreases in intensity and shifts toward 820 cm^{-1} gradually. In the melting temperature region, however, there is no band shift but the exchange of the crystalline band at 820 cm^{-1} and the amorphous band at 835 cm^{-1} with an isosbestic point. The appearance of the

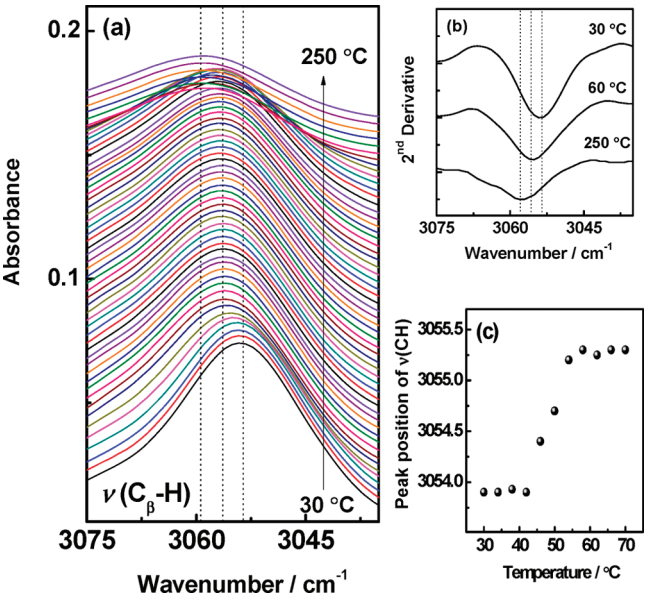

Figure 8. (a) Temporal IR spectral changes in the C_β—H stretching vibration region during the heating process of slowly crystallized P3HT from 30 to 250 at 4 °C intervals. These spectra are displayed in a stacked way. (b) Second derivatives of the spectra measured before and after the crystal-to-crystal phase transition and in the molten state. (c) Peak position of the C_β—H stretching vibration band as a function of temperature in the region of 30—70 °C.

isosbestic point suggests that there is a typical first-order phase transition for the melting process of P3HT.[30]

Yazawa et al. had investigated the thermal behavior of solution-cast P3HT film by temperature-dependent IR spectroscopy, and they assigned two bands (820 and 832 cm^{-1}) to plastic crystal and amorphous portions, respectively.[31] During heating above room temperature, they just found that there is a band shift from 820 to 832 cm^{-1} around the melting temperature of 222 °C. It should be mentioned that their sampling method is similar to ours for preparing the sample P3HT-FE, which also demonstrates the characteristic band at 820 cm^{-1}. Herein, our observations strongly indicate that the endothermic peak around 54 °C observed in DSC heating trace for slowly crystallized P3HT sample can be ascribed to the phase transition from form I′ (characterized by the band at 823 cm^{-1}) to form I (characterized by the band at 820 cm^{-1}).

As discussed previously, the peak position of the C_β—H out-of-plane deformation mode is related to the different π—π interaction modes between the neighbored conjugated planes. Figure 7a implies that the π—π stacking mode changes in the low-temperature phase transitional region. For understanding the physical meaning of the red shift for this vibration mode, we further examined the spectral behavior of C_β—H stretching mode during the heating process of P3HT form I′ crystal.

3080—3020 cm^{-1} Region: C_β—H Stretching Mode. Figure 8a shows temperature-dependent spectral changes of the C_β—H stretching mode in the 3080—3020 cm^{-1} region. In this spectral region, only one single band located around 3054 cm^{-1} can be identified. With increasing temperature from 30 to 250 °C, it is interesting to find that there are abrupt blue shifts for this mode both in the temperature region of form I′-to-form I transition and in the melting temperature region. Several selected second-derivative spectra measured at denoted temperatures as depicted

dx.doi.org/10.1021/ma2017106 |*Macromolecules* 2011, 44, 9341–9350

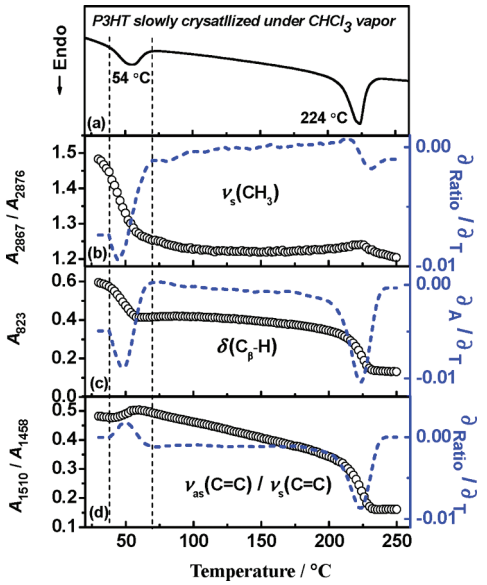

Figure 9. DSC heating trace (a) and the corresponding spectral changes associated with end methyl stacking characterized by the intensity ratio of the 2867 cm^{-1} band to 2876 cm^{-1} band (A_{2867}/A_{2876}) (b), $\pi-\pi$ stacking mode of form I′ characterized by the intensity of 823 cm^{-1} band (A_{823}) (c), and conjugated chain length characterized by intensity ratio of the 1510 cm^{-1} to 1458 cm^{-1} bands (A_{1510}/A_{1458}) (d) for P3HT-SE. The corresponding first-derivative curves of the spectral changes in (b)−(d) are also included with dashed lines.

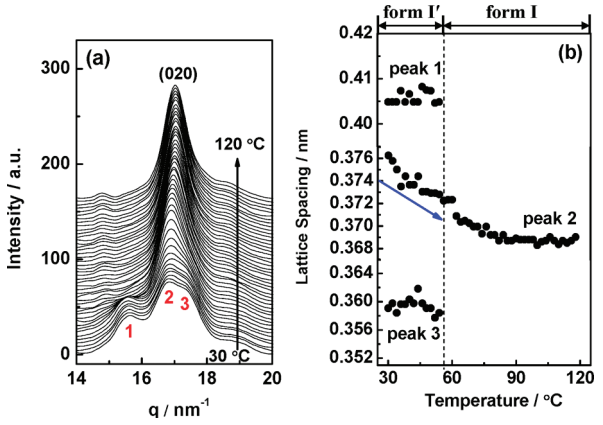

Figure 10. (a) Temperature-dependent WAXD profiles measured in transmission mode for P3HT-SE displayed from 30 to 120 at 2 °C intervals. Bragg reflections measured at 30 °C in the q region of 14−20 nm^{-1} are numbered from low to high scattering vector. (b) Temperature dependence of the lattice spacing reflected by peak 1, peak 2, and peak 3 in the region of 30−120 °C.

in Figure 8b exhibit the blue shifts mentioned above, although the shifts themselves are not so prominent. The peak position of this mode as a function of temperature in the region of 30 to 70 °C is displayed in Figure 8c. Clearly, the blue shift of this mode from 3054.0 to 3055.5 cm^{-1} demonstrates as S curve in the temperature region corresponding to the crystal-to-crystal (form I′-to-form I) phase transition very well.

It is known that the band shift can be directly correlated with the level of specific molecular interactions, such as hydrogen bonding and dipole−dipole interactions.[32−35] Specially, for various vibration modes that associated with inter- or intramolecular interaction, the band shift direction can be opposite as reported in the literature. For example, as part of the discussion for the hydrogen bonding in polyamide, the blue shift of the N−H stretching mode and the red shift of the N−H in-plane deformation mode with temperature are attributed to the decrease in the average hydrogen bond strength.[36] Considering the similar nature of the molecular interactions between the $\pi-\pi$ interaction and the hydrogen-bonding interaction, the red shift of the C_β−H out-of-plane deformation mode accompanied by the blue shift of the corresponding stretching mode occurred in the form I′-to-form I transition may also reflect the consistent change of the $\pi-\pi$ interaction.

3.4. Structural Origin of the Low-Temperature Endothermic Peak around 54 °C. In the present work, the endothermic peak around 54 °C for the sample P3HT-SE can be clearly associated with the phase transition from form I′ to form I. For clarifying this point, we summarized the DSC heating curve and the corresponding structural changes derived from previous IR analysis in Figure 9. Moreover, temperature-dependent WAXD measurement was also employed for showing the corresponding change of crystal lattice.

As shown in Figures 9a and 9b, corresponding to the phase transition temperature from 30 to 60 °C, there is abrupt change for the end methyl stacking characterized by the intensity ratio of A_{2867}/A_{2876}. Moreover, the WAXD data indicate that the peak position of (100) diffraction shifts to lower q side upon heating (data not shown). Accordingly, in the form I′-to-form I transition, the disordering of the end methyl packing as well as the increasing interlayer distance along the a-axis can be concluded. With further analysis, the disordering of end CH_3 group as denoted in Figure 9b seems to start at the lower temperature than that of the changes of $\pi-\pi$ stacking mode and conjugated chain length as denoted in Figures 9c and 9d (the structural change as denoted in Figure 9d will be discussed later). This observation may suggest that the phase transition of P3HT form I′-to-form I is triggered by the disordering of closely packed end CH_3 group.

As shown in Figure 9c, the sharp intensity change of the band at 823 cm^{-1} characteristic of P3HT form I′ is used to indicate that corresponding to the endothermic behavior around 54 °C, the $\pi-\pi$ stacking mode also changes. Actually, it is interesting to find that the red shift of the C_β−H out-of-plane deformation mode ($\delta(C_\beta-H)$) accompanied by the blue shift of the corresponding stretching mode ($\nu(C_\beta-H)$) occur in the form I′-to-form I transition as mentioned previously.

In our case, the blue shift of the $\nu(C_\beta-H)$ in the melting region around 220 °C (shown in Figures 8a and 8b) should be associated with the collapse of the crystal lattice, which is triggered by the weakening of the $\pi-\pi$ interaction. Similarly, the blue shift of this vibration mode as well as the red shift of the $\delta(C_\beta-H)$ in the form I′-to-form I transition should also reflects the decreasing of the $\pi-\pi$ interaction strength. Then, what induces the weakening of the $\pi-\pi$ interaction?

Obviously, the enlarged $\pi-\pi$ stacking distance should be considered first. Figure 10 shows the evolution of WAXD profiles and the change of corresponding crystal lattice occurring in the region of 30−120 °C for P3HT-SE. With increasing temperature, the multiple diffraction peaks in the q region of 14−20 nm^{-1} for form I′ transform to the single (020) diffraction of form I gradually. This observation supports our conclusion derived from the IR data that P3HT form I′ modification transfers to form I upon heating, the temperature region of which is around 54 °C.

dx.doi.org/10.1021/ma2017106 |Macromolecules 2011, 44, 9341–9350

Scheme 4. Schematic Drawing of the P3HT Crystal Structure along the *a*- and *b*-Axes Based on Refs 11 and 16

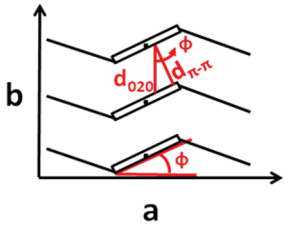

More importantly, as denoted in Figure 10b, the d_{020} spacing reflected by peak 2 decreases in the region of 30−54 °C. With further heating, this distance almost keeps constant. The observation is in contrast to the general conception that the lattice spacing increases as the result of the crystal lattice expansion under heating. Actually, the shrinking of P3HT nanocrystal along the *b*-axis was also observed by several groups.[6,37] Herein, the decreasing of d_{020} spacing seems to be contradicting with the result that the $\pi-\pi$ interaction turns to weak.

Very recently, it is reported that the thermodynamically stable P3HT stacking structure is a tilted one.[11,16] The angle ϕ between the plane of the conjugated thiophene rings and the *a*-axis as defined in Scheme 4 lies in the region of 26°−30°. Under such case, the interplanar $\pi-\pi$ stacking distance ($d_{\pi-\pi}$) is shorter than the stacking period of successive backbones along the *b*-axis (d_{020}). As depicted in Scheme 4, the relationship between these parameters can be expressed as follows:

$$d_{\pi-\pi} = d_{020} \cos \phi \quad (1)$$

Based on eq 1, the strength of the $\pi-\pi$ interaction is affected not only by the *b*-axis length but also by the degree of the tilting. Considering that the d_{020} spacing is decreased in the phase transitional process, the weakening of the $\pi-\pi$ interaction, that is, the increased $d_{\pi-\pi}$ spacing, should be contributed from the decreased angle ϕ. Dag et al. have pointed out that the main driving force for such tilted structure comes from the alkyl side-chain interactions, which can pull the backbones out of their optimal stacking positions.[16] As displayed in Figure 9, the disordering of the end methyl stacking occurs first upon heating the P3HT form I′ . Therefore, it is reasonable to propose that the decrease in tilted angel ϕ may be the reason for the weakening of the $\pi-\pi$ interaction during the form I-to-from I phase transition at low temperature.

Finally, we examine the effect of thermal annealing on the conjugated length of backbones of P3HT because it acts as the important factor for influencing the conductivity or charge transfer mobility. In order to clarify this point, the intensity ratio (A_{1510}/A_{1458}) of the C═C antisymmetric bands at 1510 cm^{-1} and C═C symmetric band at 1458 cm^{-1} is plotted against temperature in Figure 9d. According to Furukawa et al., this intensity ratio increases with the increasing of the average conjugation length of polythiophene.[38] Trznadel et al. also found the relative intensity of the 1510 cm^{-1} band increases with increasing M_n of regioregular poly(3-hexylthiophene).[39] Thus, the intensity ratio A_{1510}/A_{1458} can be used to characterize the effective conjugation length (ECL). As shown in Figure 9d, this ratio increases in the low temperature region of 30 to 60 °C, whereas it decreases in the melting temperature region of

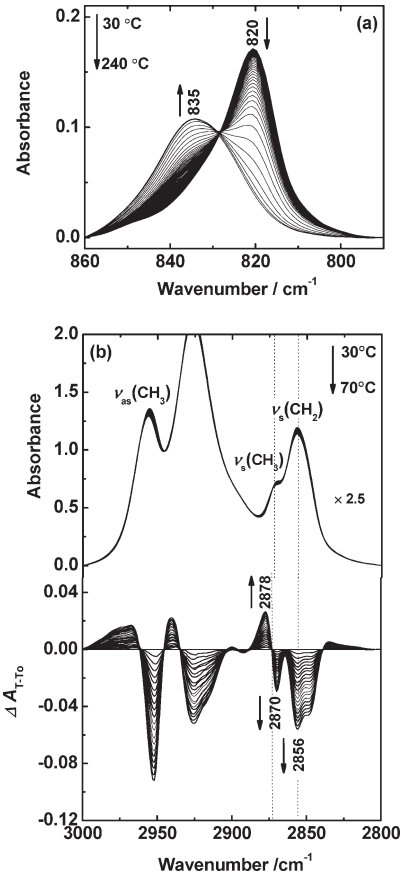

Figure 11. (a) IR spectral changes in the $C_\beta-H$ out-of-plane deformation band region during the heating process of the fast crystallized P3HT from 30 to 240 at 4 °C intervals. (b) IR spectral changes in the C−H stretching vibration region from 30 to 70 at 2 °C intervals and the corresponding difference spectra obtained by the subtraction of the initial spectrum measured at 30 °C are shown in the upper and lower part, respectively.

200−230 °C. This result suggests that the ECL of P3HT-SE increases slightly in the transitional process of form I′-to-form I.

In the field of organic electronic applications, annealing treatment between T_g and T_m is often performed on P3AT film.[40,41] Our previous work indicated that the backbone planarity is destroyed in the form I′-to-form I transition of P3BT, which implies that annealing treatment on P3BT is unfavorable for the improved conductivity.[42] However, in this work, the increased ECL occurred in P3HT form I′-to-form I transition indicate that high-temperature annealing will be helpful for improving the conductivity of the slowly evaporated P3HT film.

It should be recognized that we just provide a roughly structural model to explain our experimental data. Our understating on the accurate crystal structure of the new crystal modification reported here is very limited at the current stage. However, after comprehensively considering the data of DSC, WAXD, and IR spectroscopy, it is indeed clear that the endothermic peak around 54 °C as shown in Figure 1a is assigned to the form I′-to-form I transition. Then, how does one explain the subtle changes in P3HT-FE endothermic peak around 64 °C which is also observed by many other groups and have a detailed explanation? For this transition, is there any crystalline structure change?

dx.doi.org/10.1021/ma2017106 |*Macromolecules* 2011, 44, 9341–9350

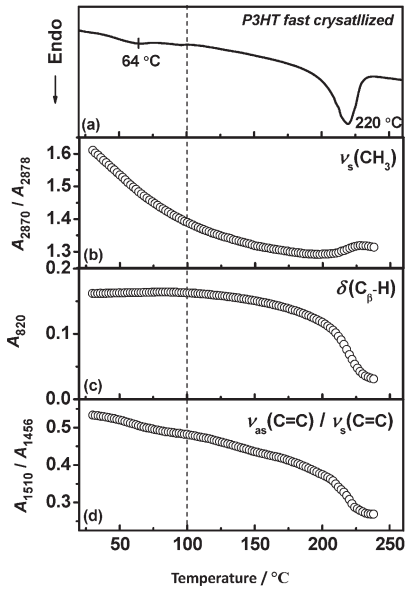

Figure 12. DSC heating trace (a) and the corresponding spectral changes associated with end methyl stacking characterized by the intensity ratio of the 2870 cm^{-1} band to 2878 cm^{-1} band (A_{2870}/A_{2878}) (b), $\pi-\pi$ stacking mode of form I characterized by the intensity of 820 cm^{-1} band (A_{820}) (c), and conjugated chain length characterized by intensity ratio of the 1510 cm^{-1} to 1456 cm^{-1} (A_{1510}/A_{1456}) (d) for the fast evaporated P3HT film.

Usually, the low-temperature endothermic peak around 60 °C in P3AT was ascribed to the melting or disordering of alkyl side chains.[3,22] For example, as mentioned in the Introduction, Thelakkat et al. observed that several ($hk0$) diffractions start to disappear with increasing temperature above 60 °C for P3HT sample with well-defined molecular weight, and they proposed that the disappearing of these ($hk0$) diffractions was attributed to the "melting of hexyl side chains".[3] Their results suggest that the hexyl side chains in P3HT crystal take the ordered extended chain conformation, which is consistent with the widely accepted packing model of P3ATs. In contrast, Kline et al. and Yazawa et al. recently concluded from spectroscopic experiments that the side chains of P3HT are disordered at room temperature.[43,44] Therefore, there is no complete agreement on this point in the literature.

For addressing these issues, the temperature-dependent IR spectroscopy was also performed for P3HT-FE. The *in situ* spectral change of the $C_\beta-H$ out-of-plane mode and the C−H stretching mode associated with the stacking structure are plotted in Figures 11a and 11b, respectively. Comparing to the temperature-dependent IR data of P3HT-SE, most obviously spectral difference lies in the region of 860−800 cm^{-1}. In the whole heating process, the $C_\beta-H$ out-of-plane mode for P3HT-FE as shown in Figure 11a only exhibit the melting behavior characterized by the exchange between the 820 cm^{-1} band and the 835 cm^{-1} band. Also as shown in Figure 11b, upon heating from 30 to 70 °C, the band shifting to higher wavenumber is only discernible on the $\nu_s(CH_3)$ characterized by the appearance of the positive peak at 2878 cm^{-1} and the negative peak at 2870 cm^{-1}.

The quantitative spectral changes of the fast evaporated sample are plotted in Figure 12. Corresponding to the subtle endothermic behavior around 64 °C as shown in Figure 12a, the end methyl stacking characterized by the intensity ratio of the 2870 cm^{-1} band to 2878 cm^{-1} band (shown in Figure 12b) seems to exhibit weak disordering. However, different from the sample P3HT-SE, there is no obvious structure rearrangement on the conjugated backbones, that is, the change of $\pi-\pi$ stacking as indicated in Figure 12c and the change of effective conjugation length as shown in Figure 12d. According to these data, it is found that both the phase transition around 54 °C and that around 64 °C involve a structural disordering process of the alkyl side chains. However, in contrast to the 64 °C phase transition, there is obvious structural rearrangement on the conjugated backbone chain (changes in $\pi-\pi$ stacking and effective conjugated length) except for the disordering of alky chains for the 54 °C phase transition as evidenced by the temperature-dependent IR and WAXD data. Therefore, we assigned the endothermic peak around 54 °C to the form I′-to-form I transition, and we think that it has the different nature with that of the reported phase transition around 64 °C.

4. CONCLUSION

Chloroform is a good solvent for rr-P3HT active layers in field effect transistors. However, its rapid evaporation rate resulted by the low boiling point limit the crystallization time of P3HT during the solution-coating process. Herein, by controlling the evaporation rate of chloroform solvent at low temperature, we obtained a new crystal modification named as form I′ as evidenced from the DSC measurement, X-ray diffraction, and infrared spectroscopy. Compared to the more disordered form I commonly obtained from fast solvent evaporation rate or from melt-crystallization, form I′ modification presents some analogies but significant differences.

It is interesting to find that there is a distinct endothermic peak around 54 °C in the DSC heating curve of rr-P3HT form I′ crystal. The nature of the structural transition corresponding to this endothermic peak for form I′ is investigated in detail by temperature-dependent IR combined with the *in situ* WAXD measurement. It is found that, during the heating process, there is a phase transition from form I′ to form I in the region of 30−60 °C. Our analysis indicates that, with heating in this temperature region, the packing of end CH_3 groups in form I′ experiences an obvious disordering process. Meanwhile, both the IR and synchrotron WAXD data suggest that there is a change in the $\pi-\pi$ stacking modes of conjugated backbone chain during the phase transitional process from form I′ to form I. It should be pointed out that our understating on the accurate crystal structure of the new crystal modification reported here is very limited at the current stage. For clarifying the practical crystal structure of P3HT form I′, more effort is needed for further research.

AUTHOR INFORMATION

Corresponding Author

*Fax: +86-532-84022791. E-mail: zjm@qust.edu.cn (J.Z.), dyx@qust.edu.cn (Y.D.).

ACKNOWLEDGMENT

The financial support from Taishan Mountain Scholar Constructive Engineering Foundation (TS20081120) and Natural Science Fund for Distinguished Young Scholars of Shandong Province (JQ200905) is greatly appreciated. Jianming Zhang thanks the Alexander von Humboldt foundation for supporting

his research stay at the Max Planck Institute for Polymer Research in Mainz, Germany.

REFERENCES

(1) Hugger, S.; Thomann, R.; Heinzel, T.; Thurn-Albrecht, T. *Colloid Polym. Sci.* **2004**, *282*, 932–938.
(2) Joshi, S.; Grigorian, S.; Pietsch, U.; Pingel, P.; Zen, A.; Neher, D.; Scherf, U. *Macromolecules* **2008**, *41*, 6800–6808.
(3) Wu, Z. Y.; Petzold, A.; Henze, T.; Albrecht, T. T.; Lohwasser, R. H.; Sommer, M.; Thelakkat, M. *Macromolecules* **2010**, *43*, 4646–4653.
(4) Brinkmann, M.; Rannou, P. *Macromolecules* **2009**, *42*, 1125–1130.
(5) Sirringhaus, H.; Brown, P. J.; Friend, R. H.; Nielsen, M. M.; Bechgaard, K.; Langeveld-Voss, B. M. W.; Spiering, A. J. H.; Janssen, R. A. J.; Meijer, E. W.; Herwig, P.; de Leeuw, D. M. *Nature* **1999**, *401*, 685–688.
(6) Zen, A.; Saphiannikova, M.; Neher, D.; Grenzer, J.; Grigorian, S.; Pietsch, U.; Asawapirom, U.; Janietz, S.; Scherf, U.; Lieberwirth, I.; Wegner, G. *Macromolecules* **2006**, *39*, 2162–2171.
(7) Zen, A.; Pflaum, J.; Hirschmann, S.; Zhuang, W.; Jaiser, F.; Asawapirom, U.; Rabe, J.; Scherf, U.; Neher, D. *Adv. Funct. Mater.* **2004**, *14*, 757–764.
(8) DeLongchamp, D. M.; Kline, R. J.; Fischer, D. A.; Richter, L. J.; Toney, M. F. *Adv. Mater.* **2011**, *23*, 319–337.
(9) Chang, J. F.; Sun, B.; Breiby, D. W.; Nielsen, M. M.; Solling, T. I.; Giles, M.; McCulloch, I.; Sirringhaus, H. *Chem. Mater.* **2004**, *16*, 4772–4776.
(10) Pankaj, S.; Beiner, M. B. *Soft Matter* **2010**, *6*, 3506–3516.
(11) Kayunkid, N.; Uttiya, S.; Brinkmann, M. *Macromolecules* **2010**, *43*, 4961–4967.
(12) Hsu, W. P.; Levon, K.; Ho, K. S.; Myerson, A. S.; Kwei, T. K. *Macromolecules* **1993**, *26*, 1318–1323.
(13) Jordan, E. F.; Feldeise, D. W.; Wrigley, A. N. *J. Polym. Sci., Part A-1* **1971**, *9*, 1835–1851.
(14) Hempel, E.; Huth, H.; Beiner, M. *Thermochim. Acta* **2003**, *403*, 105–114.
(15) Mierzwa, M.; Floudas, G.; Stepanek, P.; Wegner, G. *Phys. Rev. B: Condens. Matter Mater. Phys.* **2000**, *62*, 14012–14019.
(16) Dag, S.; Wang, L. W. *J. Phys. Chem. B* **2010**, *114*, 5997–6000.
(17) Arosio, P.; Moreno, M.; Famulari, A.; Raos, G.; Catellani, M.; Meille, S. V. *Chem. Mater.* **2009**, *21*, 78–87.
(18) Pascui, O. F.; Lohwasser, R.; Sommer, M.; Thelakkat, M.; Albrecht, T. T.; Saalwachter, K. *Macromolecules* **2010**, *43*, 9401–9410.
(19) Zhang, J. M.; Tashiro, K.; Tsuji, H.; Domb, J. A. *Macromolecules* **2008**, *41*, 1352–1357.
(20) Prosa, T. J.; Winokur, M. J. *Macromolecules* **1996**, *29*, 3654–3656.
(21) McCullough, R. D.; Nagle, S. T.; Williams, S. P.; Lowe, R. D.; Jayaraman, M. *J. Am. Chem. Soc.* **1993**, *115*, 4910–4911.
(22) Tashiro, K.; Ono, K.; Mipagawa, Y.; Kobayashi, M.; Kawai, T.; Yoshino, Y. *J. Polym. Sci., Part B: Polym. Phys.* **1991**, *29*, 1223–1233.
(23) Zerbi, G.; Chierichetti, B. *J. Chem. Phys.* **1991**, *94*, 4646–4658.
(24) Yazawa, K.; Inoue, Y.; Yamamoto, T.; Asakawa, N. *Phys. Rev. B* **2006**, *74*, 094204–1−12.
(25) Curtis, M. D.; Nanos, J. I.; Moon, H.; Jahng, W. S. *J. Am. Chem. Soc.* **2007**, *129*, 15072–15084.
(26) Bolognesi, A.; Porzio, W.; Provasoli, F. *Makromol. Chem.* **1993**, *194*, 817–827.
(27) Winokur, M. J.; Spiegel, D.; Kim, Y.; Hotta, S.; Heeger, A. J. *Synth. Met.* **1989**, *28*, 419–426.
(28) Schachtschneider, J. H.; Snyder, R. G. *Spectrochim. Acta* **1963**, *19*, 85–116.
(29) Schachtschneider, J. H.; Snyder, R. G. *Spectrochim. Acta* **1963**, *19*, 117–168.
(30) Flory, P. J.; Garrett, R. R. *J. Am. Chem. Soc.* **1958**, *80*, 4836–4845.
(31) Yazawa, K.; Inoue, Y.; Yamamoto, T.; Asakawa, N. *J. Phys. Chem. B* **2008**, *112*, 11580–11585.
(32) Banno, M.; Ohta, K.; Yamaguchi, S.; Hirai, S.; Tominaga, K. *Acc. Chem. Res.* **2009**, *42*, 1259–1269.
(33) Coleman, M. M.; Lee, K. H.; Skrovanek, D. J.; Painter, P. C. *Macromolecules* **1986**, *19*, 2149–2157.
(34) Choperena, A.; Painter, P. C. *Macromolecules* **2009**, *42*, 6159–6165.
(35) Huang, H.; Malkov, S.; Coleman, M.; Painter, P. *J. Phys. Chem. A* **2003**, *107*, 7697–7703.
(36) Skrovanek, D. J.; Howe, S. E.; Painter, P. C.; Coleman, M. M. *Macromolecules* **1985**, *18*, 1676–1683.
(37) Joshi, S.; Grigorian, S.; Pietsch, U. *Phys. Status Solidi* **2008**, *205*, 488–496.
(38) Lu, G. H.; Li, L. G.; Yang, X. N. *Macromolecules* **2008**, *41*, 2062–2070.
(39) Furukawa, Y.; Agimoto, M.; Harada, I. *Synth. Met.* **1987**, *18*, 151–156.
(40) Trznadel, M.; Pron, A.; Zagorska, M.; Chrzaszcz, R.; Pielichowski, J. *Macromolecules* **1998**, *31*, 5051–5058.
(41) Gurau, M. C.; Delongchamp, D. M.; Vogel, B. M.; Lin, E. K.; Fischer, D. A.; Sambasivan, S.; Richter, L. J. *Langmuir* **2007**, *23*, 834–842.
(42) Yuan, Y.; Zhang, J. M.; Sun, J. Q. *Macromolecules* **2011**, *44*, 6128–6135.
(43) Kline, R. J.; Delongchamp, D. M.; Fischer, D. A.; Lin, E. K.; Richter, L. J.; Chabinyc, M. L.; Toney, M. F.; Heeney, M.; McCulloch, L. *Macromolecules* **2007**, *40*, 7960–7965.
(44) Yazawa, K.; Inoue, Y.; Shimizu, T.; Tansho, M.; Asakawa, N. *J. Phys. Chem. B* **2010**, *114*, 1241–1248.